Journal of Advanced Concrete Technology Vol. 20, 507-524, August 2022 / Copyright © 2022 Japan Concrete Institute

Scientific paper

Simplified Three-Parameter Kinematic Theory for Shear Strength of Short Reinforced Concrete Walls

Eissa Fathalla[1*] and Boyan Mihaylov[2]

Received 13 March 2022, accepted 25 July 2022 doi:10.3151/jact.20.507

Abstract

In this paper, a simplified model is proposed for the shear strength of short shear walls based on the original three-parameter kinematic theory (3PKT). The model is built on first principles – compatibility of deformations, constitutive relationships and equilibrium – and aims to combine simplicity and accuracy for structural assessment applications. The model focuses on shear failures along diagonal cracks, while other failure modes such as sliding shear, out-of-plane instability, or detailing/lap splice failures need to be evaluated separately. The simplified 3PKT is validated with 29 specimens with a wide range of properties and is compared to the ASCE (ASCE 2014) and Japanese (AIJ 2001) seismic code shear provisions. It is shown that the model captures well the effect of all key test variables, and significantly reduces the conservatism and scatter of the code strength predictions. It is also shown that the proposed approach can be particularly helpful in the assessment of structures with less-than-minimum shear reinforcement to avoid costly and disruptive strengthening interventions.

1. Introduction

While the flexural behavior of slender shear walls is well understood, the response of short shear-dominated walls is still under investigation due to the complexity of the shear-resisting mechanisms and their interactions. This paper aims to propose a rational mechanical model for the shear strength of short shear walls with aspect ratios $a/h \leq 3.0$, where brittle shear failures occur before the yielding of the flexural reinforcement.

Several approaches with different levels of complexity have been proposed for predicting the shear strength of shear walls. The simplest engineering approach is the use of empirical or semi-empirical equations provided in design codes such as the ASCE code (ASCE 2014) or AIJ code (AIJ 2001). While such equations are convenient, they typically feature significant conservatism, which can lead to overdesign of newly constructed walls or, more importantly, to costly retrofit of existing structures. Other simple models have been proposed (Pristely 2007; Biskinis and Fardis 2010; CEN 2005; Beyer *et al.* 2011), where all the plastic deformations are lumped in a plastic hinge at the base of the wall (plastic hinge models). This approach is based mainly on flexural behavior, and it is not well suited for the modelling of brittle shear failures of short walls occurring before yielding of the flexural reinforcement. To capture such failures, researchers have also proposed truss (or strut-and-tie) models (Mazars *et al*. 2002; Park and Eom 2007; Panagiotou *et al*. 2012), where the wall is discretized into a number of one-dimensional vertical, horizontal, and inclined truss elements (struts for concrete in compression and ties for reinforcement in tension). The struts and ties are assigned nonlinear load-displacement relationships based on the properties of the concrete and reinforcement. Several difficulties are encountered in this approach, as for example the proper selection of the layout and dimensions of the truss members, and in particular, the struts. Moreover, the critical shear cracks are not modelled explicitly in truss models; therefore, this approach is not suitable for evaluating aggregate interlock resistance and crack widths. The main limitation of truss models however is that they are not applicable to brittle structures with less-than-minimum shear reinforcement. In order to take into account the complex behavior of cracked reinforced concrete, nonlinear finite element (FE) formulations have also been used to model shear walls (Bažant and Oh 1985; Vecchio and Collins 1986; Vecchio 2000; Kagermanov and Ceresa 2016). However, while FE models can produce adequate results of strength and deformations when applied properly, they require considerable time to conduct appropriate modelling, in addition to, the need for engineers with strong FE background. Therefore, there remains a need for simplified mechanical models for the engineering practice to reliably predict the ultimate behavior of short shear-dominated walls.

A suitable basis for addressing this need is provided by a three-parameter kinematic theory (3PKT) for shear-

[1]Postdoctoral Researcher, Urban and Environmental Research Unit (UEE), University of Liège, Building B52, Quartier Polytech 1, Allée de la Découverte 9, B-4000 Liège, Belgium, and Assistant Professor, Structural Engineering Department, Cairo University, Giza 12613, Egypt.
*Corresponding author, *E-mail*: mmeissa@uliege.be
[2]Assistant Professor, Urban and Environmental Research Unit (UEE), University of Liège, Building B52, Quartier Polytech 1, Allée de la Découverte 9, B-4000 Liège, Belgium.

dominated walls (Mihaylov *et al*. 2016), which was developed from an earlier two-parameter kinematic theory (2PKT) for deep beams (Mihaylov *et al.* 2013). This approach is built on a kinematic description of the deformation patterns of diagonally cracked walls with rectangular sections, and also includes equilibrium conditions and constitutive relationships for the shear mechanisms in the wall. It was developed to simulate the complete nonlinear response of walls by using three degrees of freedom (DOFs), capturing both global and local deformations from zero load up to failure. The adequacy of the 3PKT has been demonstrated via comparisons with a large number of tests (Mihaylov *et al.* 2016; Tatar and Mihaylov 2019). Because the 3PKT is based on first principles, it allows to be either extended or simplified depending on the goal of the analysis.

In this paper, the 3PKT is simplified to focus solely on the shear strength (peak response) of short shear-dominated walls. While the complete nonlinear response of walls can be of interest, it is the shear strength that is typically sufficient for safety verifications. For such calculations, it is preferred to use either closed-form equations or simple iterative procedures, rather than the complete nonlinear analysis offered by the original 3PKT. The proposed simplified 3PKT approach is validated with a wide range of shear walls from past experiments, and the results demonstrate the robustness of the model. Moreover, different test variables of shear walls are studied based on the simplified 3PKT to understand their impact on the shear strength.

This proposed simplified model allows engineers to conduct safety checks on the shear strength of walls by simple calculations since it is based on only three DOFs without the need of FE modeling and nonlinear simulation software. However, more detailed methods can be used to check in further detail the performance and evaluate the deformations of shear-critical shear walls.

2. Original 3PKT approach of shear-dominated shear walls

The 3PKT approach (Mihaylov *et al*. 2016) is based on a kinematic model that describes the deformation field of cracked shear-dominated rectangular walls. The model has been developed based on observations and measurements from tests of walls under the combined effect of vertical and lateral loads, where the failure is governed mainly by the opening of diagonal shear cracks.

According to the 3PKT, the ultimate deformation pattern of the wall can be obtained as a superposition of three deformation fields, where each field is a function of a single DOF – see **Fig. 1(a)**. The deformation fields are marked by a straight diagonal shear crack with an inclination of α_1 with respect to the vertical axis. This crack divides the wall into two regions: a rigid block above the crack and a fan of struts below the crack. The flexural reinforcement in the fan is modelled with a vertical tie, which represents the bars in the tensile one-half of the section in terms of their area A_s and centroidal axis.

The first deformation pattern corresponds to the elongation of the vertical tie, expressed with the average strain along the tie $\varepsilon_{t,avg}$. As DOF $\varepsilon_{t,avg}$ increases, the fan

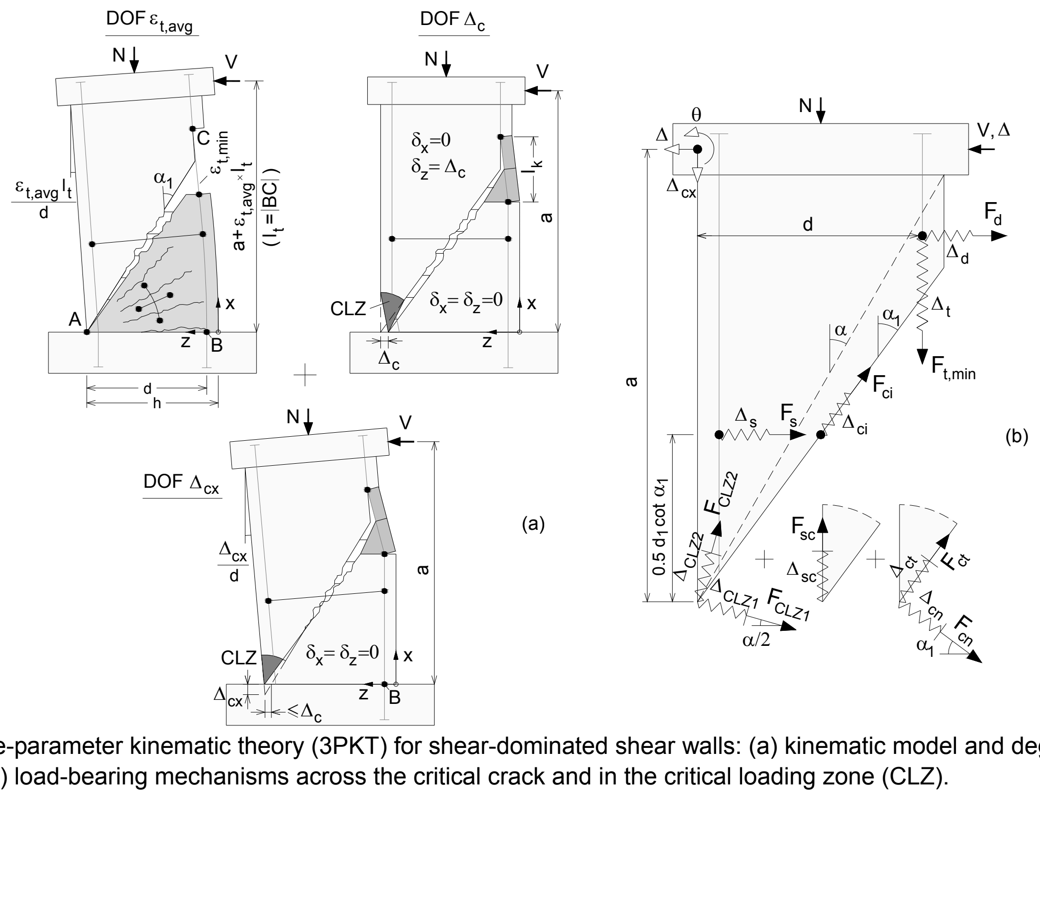

Fig. 1 Three-parameter kinematic theory (3PKT) for shear-dominated shear walls: (a) kinematic model and degrees of freedom; (b) load-bearing mechanisms across the critical crack and in the critical loading zone (CLZ).

of struts opens and the rigid block rotates about the toe of the wall (pivot A). Associated with that, the critical shear crack widens. The second deformation pattern is characterized by lateral displacement Δ_c of the rigid block with respect to the fan (DOF Δ_c). This displacement results in widening and slip displacements in the critical crack. Moreover, Δ_c is associated with compressive strains and stresses in the critical loading zone (CLZ) near the toe of the wall. The third deformation pattern is characterized by a downward displacement Δ_{cx} occurring in the CLZ, which results in rotation of the rigid block about pivot B at the bottom of the vertical tie. While DOFs $\varepsilon_{t,avg}$ and Δ_c are sufficient for the modelling of members without axial load or prestressing, DOF Δ_{cx} is necessary in the presence of axial compression N, which tends to drive the rigid block downwards. The rotation about pivot B is associated with widening and slip displacements in the critical crack. By superimposing the three deformation patterns for given values of the three DOFs, the full deformation field and crack displacements are obtained.

Moreover, the load-bearing mechanisms of the wall are modelled by nonlinear springs across the critical crack and in the CLZ – **Fig. 1(b)**. The deformations of the springs are derived from the kinematic model (compatibility of deformations) and are used together with constitutive relationships for the load-bearing mechanisms in the wall. The springs represent the tension in the flexural reinforcement (tie) $F_{t,min}$, the shear due to aggregate interlock F_{ci}, the tension is the transverse reinforcement F_s, the contact forces F_{cn} and F_{ct} (if present) between the rigid block and the fan in the vicinity of the CLZ, the dowel action of the flexural reinforcement (tie) F_d, the compression forces in the concrete of the CLZ F_{CLZ1} and F_{CLZ2}, and the compression (F_{sc}) in the vertical reinforcement in the CLZ. These forces can be evaluated for any set of DOFs $\varepsilon_{t,avg}$, Δ_c and Δ_{cx}.

In the solution procedure outlined in (Mihaylov *et al.* 2016), a lateral displacement Δ is imposed at the top of the wall, thus reducing the unknown DOFs to two. In addition, by satisfying the vertical and moment equilibrium of the forces acting on the rigid block (i.e., spring forces F_i and normal force N), the two other DOFs are determined. In a final step, the horizontal equilibrium of the rigid block is used to determine the lateral load V on the wall corresponding to the imposed lateral displacement Δ.

This approach was developed to model the complete nonlinear load-displacement response of shear-dominated walls, including the post-peak response. It is applicable to walls that fail either in shear along diagonal cracks or at the base section under the combination of flexure and shear. The failure along the diagonal cracks can occur either in a brittle manner prior to yielding of the flexural reinforcement, or in a more ductile manner after flexural yielding. However, while the 3PKT is computationally efficient and uses simple input, it still represents significant complexity for practical safety verifications. For this reason, in the following, the 3PKT is simplified to focus only on the peak response (strength) of shear walls.

3. Simplified 3PKT approach for the shear strength of shear-dominated walls

Of most interest and challenge for practical applications is the prediction of brittle shear failures along diagonal cracks. In short walls with aspect ratios $a/h \leq 3.0$, such failures occur under the complex interaction between shear, bending and axial load. Therefore, the simplified 3PKT targets namely the shear strength of walls that fail prior to yielding of the flexural reinforcement.

Figure 2 shows the geometrical properties of the kinematic model, which are adopted from the original 3PKT. The angle of the shear crack α_1 is estimated as

$$\alpha_1 = \max(\alpha, 30°), \quad \alpha = \tan^{-1}(h/a_{cl}) \tag{1}$$

where α is the angle of the diagonal of the wall region with respect to the vertical axis, h is the length of the wall, and a_{cl} is the clear height of the wall. At the top end of the critical crack, a heavily cracked zone develops with a length l_k along the vertical tie. This zone is of significance for the opening of the critical crack and for the dowel action of the vertical reinforcement. Length l_k is estimated according to Eqs. (2) to (5) taking into account the crack spacing along the vertical tie s_{cr}:

$$l_k = l_0 + \min\left[s_{cr}, d \times \left(\cot\alpha - \cot\alpha_1\right)\right] \tag{2}$$

$$l_0 = \max\left[s_{cr}, \min(1.5(h-d), d - h/2)\cot\alpha_1\right] \tag{3}$$

$$s_{cr} = \frac{0.28 d_b}{\rho_{l1}} 100 \tag{4}$$

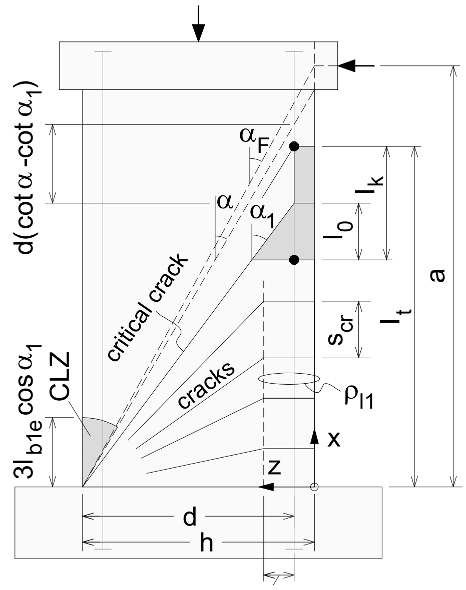

Fig. 2 Geometry of kinematic model.

$$\rho_{l1} = \frac{A_s}{b \cdot (h-d) + \min\left[1.5(h-d), d-h/2\right]}100$$
$$A_s = \frac{1}{2}\rho_l bh/100 \tag{5}$$

where d is the distance from the outer most compression fibers of the wall to the vertical tie, A_s is the area of the tie representing the reinforcement in the tensile one-half of the section (i.e., within $h/2$), d_b is the diameter of the main vertical reinforcement in the tie, b is the width of the rectangular wall section, ρ_l is the total ratio of vertical reinforcement in the section, and ρ_{l1} is the reinforcement ratio in the zone with enhanced crack control around the vertical tie. The total cracked length along the vertical tie extends from the bottom section of the wall to the top end of length l_k:

$$l_t = d/\tan\alpha_1 + (l_k - l_0) \tag{6}$$

It is along this length that the average tie strain $\varepsilon_{t,avg}$ is defined and integrated. The other important geometrical property of the kinematic model is the characteristic length of the critical loading zone l_{b1e} The CLZ is idealized as a circular sector with a radius $3l_{b1e}\cos\alpha_1$ and a center located at the compression toe of the wall. Length l_{b1e} has been derived based on comparisons with tests (Mihaylov *et al.* 2016):

$$l_{b1e} = \min\left[0.11\sqrt{a^2+h^2}, 370\,\text{mm}\right] \tag{7}$$

where a is the height of the member from the base section to the level of the lateral load.

Taking into account the above geometrical properties and the kinematics in **Fig. 1(a)**, the crack width w and the strain in the transverse reinforcement ε_v halfway along the critical crack have been derived – see Eqs. (8) to (10) (Mihaylov *et al.* 2016). Both deformations are functions of the three DOFs of the kinematic model. In the expression for w, n_{cr} takes into account the crack control in the web of the wall. In the presence of sufficient vertical reinforcement in the web (reinforcement ratio ρ_{lw}), the crack width determined from the kinematic model is divided among n_{cr} major cracks. In the expression for ε_v, the factor of 2 accounts for strain localization in the critical crack. Length d_1 in Eq. (10) is the distance from the compression edge of the wall to the farthest layer of vertical bars in the section.

$$w = \begin{bmatrix} \dfrac{\varepsilon_{t,avg} l_k h}{2\sin\alpha_1 d} \\ +\Delta_c\cos\alpha_1 \\ +\dfrac{\Delta_{cx}}{d}\left(\dfrac{h}{2\sin\alpha_1} - d\sin\alpha_1\right) \end{bmatrix} / n_{\text{cr}} \tag{8}$$

$$n_{cr} = \frac{l_k}{s_{cr}} \quad if \quad \rho_{lw} \geq 0.2\%$$
$$n_{cr} = 1.0 \quad if \quad \rho_{lw} < 0.2\% \tag{9}$$

$$\varepsilon_v = 2.0\begin{bmatrix} \left(\dfrac{\varepsilon_{t,avg} l_t}{d} + \dfrac{\Delta_{cx}}{d}\right)0.5d_1\cot\alpha_1 \\ +\Delta_c - \varepsilon_{t,avg}\dfrac{(0.5d_1\cot\alpha_1)^2}{d} \end{bmatrix} / 0.9d_1 \tag{10}$$

To simplify the 3PKT approach, it will be assumed that the concrete in the CLZ crushes at shear failure. This assumption is based on multiple test observations showing significant spalling of concrete at the toe of the wall, which occurs simultaneously with the opening of the critical diagonal crack. To reflect this observation, the strain in the CLZ at failure is estimated at ε_{CLZ}=−0.0035, which is also consistent with digital image correlation measurements from wall tests (Langer 2019). The goal of this simplification is to estimate DOFs Δ_c and Δ_{cx} at failure without the need for a complete nonlinear analysis from zero load.

Figure 3 shows the proposed simplified model of the CLZ. Strain ε_{CLZ} is oriented in the direction of the resultant force in the CLZ, F_{CLZ}, which itself is inclined at angle α_F with respect to the vertical axis. As short shear walls work predominantly in diagonal compression, angle α_F is estimated at $\tan^{-1}(h/a)$. Furthermore, the angle of force F_{CLZ} is linked to the angle of the displacement in the CLZ, Δ_{CLZ}, where Δ_{CLZ} is the resultant vector of DOFs Δ_c and Δ_{cx}. In a study on prestressed concrete deep beams, Mihaylov *et al.* (2021) have proposed the following simplified relationship between the force angle α_F and displacement angle α_Δ:

$$\alpha_\Delta = \min\left[\frac{\alpha_F}{\alpha_1} \times 90, 90°\right] \tag{11}$$

where α_1 is the angle of the critical crack [Eq. (1)]. Ac-

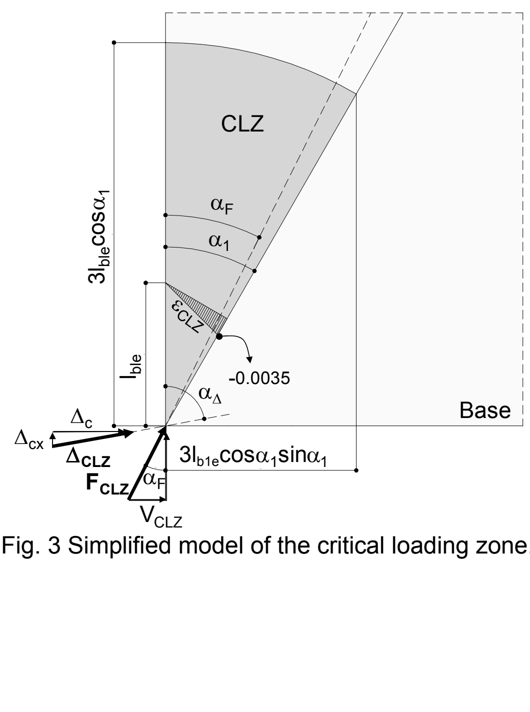

Fig. 3 Simplified model of the critical loading zone.

cording to Eq. (11), when F_{CLZ} is aligned with the critical crack (i.e., $\alpha_F \approx \alpha_1$), Δ_{CLZ} is horizontal. This limit case is consistent with test observations in deep members without axial load or prestressing (Mihaylov *et al.* 2013).

To proceed with the evaluation of DOFs Δ_c and Δ_{cx}, the CLZ displacement in the direction of force F_{CLZ} is obtained by multiplying strain ε_{CLZ} by the radius of the critical loading zone $3l_{b1e}\cos\alpha_1$. This displacement represents the projection of Δ_{CLZ} on the direction of F_{CLZ}, and therefore Δ_{CLZ} is obtained as:

$$\Delta_{CLZ} = \frac{\varepsilon_{CLZ} \times 3l_{b1e}\cos\alpha_1}{\cos(\alpha_\Delta - \alpha_F)} \tag{12}$$

In turn, when Δ_{CLZ} is projected on the horizontal and vertical axes, the two DOFs of the kinematic model at shear failure are obtained:

$$\Delta_c = \Delta_{CLZ}\sin\alpha_\Delta, \quad \Delta_{cx} = \Delta_{CLZ}\cos\alpha_\Delta \tag{13}$$

Note that these DOFs are determined in advance based on the geometry of the wall without the need for iterative calculations.

To calculate the third DOF of the kinematic model $\varepsilon_{t,avg}$ and the shear strength of the wall, it is necessary to model the shear mechanisms in the CLZ and along the critical crack. To simplify the model further, simpler equations are proposed as compared to the complete nonlinear relationships of the springs used in the original 3PKT. There are four main shear mechanisms in shear walls that are taken into account in the simplified 3PKT as follows.

- Shear carried in the critical loading zone V_{CLZ}

The average compressive stress in the CLZ in the direction of force F_{CLZ} is evaluated at $1.48f_c^{0.8}$ as proposed in (Mihaylov *et al.* 2021). This value is obtained for a maximum strain ε_{CLZ}=−0.0035 by using an appropriate stress-strain relationship for the concrete in compression (Popovics 1973). The critical section of the CLZ is located at a vertical distance of l_{b1e} from the compression toe of the wall (**Fig. 3**), and the width of this section is $l_{b1e}sin\alpha_1$. When the area of the section $(l_{b1e}\sin\alpha_1)b$ is multiplied by the average stress $1.48f_c^{0.8}$, force F_{CLZ} is obtained. This force is projected on the horizontal axis to obtain the shear carried in the CLZ:

$$V_{CLZ} = l_{ble}\sin\alpha_1 b \times 1.48 f_c'^{0.8}\sin\alpha_F \tag{14}$$

- Shear carried by aggregate interlock V_{ci}

The aggregate interlock shear stress v_{ci} is evaluated based on the crack width w by using an expression proposed by Vecchio and Collins (1986). Stress v_{ci} is integrated along the critical crack to obtain the shear resistance provided by aggregate interlock:

$$V_{ci} = \upsilon_{ci} b d_1$$
$$\upsilon_{ci} = \frac{0.18\sqrt{f_c'}}{0.31 + 24w/\left(a_g + 16\right)} \quad \text{(MPa)} \tag{15}$$

where w (mm) is calculated from Eq. (8) and a_g (mm) is the maximum size of coarse aggregates in the concrete.

- Shear carried by transverse reinforcement V_s

The stress in the transverse reinforcement f_v is evaluated based on strain ε_v from Eq. (10) by using an elastic-perfectly-plastic stress-strain relationship for the steel. Stress f_v is multiplied by the area of activated stirrups along the critical crack to obtain the shear carried by the stirrups (Mihaylov *et al.* 2016):

$$V_s = \frac{\rho_v}{100} b \cdot \max\begin{bmatrix} d_1\cot\alpha_1 - 1.5l_{b1e} - \dfrac{dl_0}{d_1}, \\ 0.5d_1\cot\alpha_1 \end{bmatrix} f_v \tag{16}$$

where ρ_v is the transverse reinforcement ratio. The expression in the brackets represents the height along the wall within which the transverse reinforcement is considered effective.

- Shear carried by dowel action of the flexural reinforcement V_d

The dowel action of the flexural tension reinforcement (tie) develops within length l_k and is associated with the transverse displacement Δ_c. The bar-dowels are modelled as fixed-fixed beam elements with a length l_k, which work in double curvature with zero bending moment halfway along l_k. The ultimate capacity of the bar-dowels is governed by the formation of plastic hinges at the two ends of l_k. Based on these assumptions, the following expression for the shear carried by the dowels has been derived (Mihaylov *et al.* 2013):

$$V_d = n_b f_y \left[1 - \left(\frac{\varepsilon_{t,avg}}{f_y / E_s}\right)^2\right] \frac{d_b^{\,3}}{3l_k} \tag{17}$$

where the expression in the square brackets is minimum zero. As evident from this equation, V_d depends on the unknown DOF $\varepsilon_{t,avg}$. The larger is the tensile strain in the bar-dowels, the lower is the moment capacity of the plastic hinges, and therefore the weaker is the dowel action. Note also that DOF $\varepsilon_{t,avg}$ similarly affects shear contributions V_{ci} and V_s via the crack width w and stirrups strain ε_v, respectively [Eqs. (8) to (10)].

The four shear strength contributions are added up to express the shear resistance of the wall:

$$V = V_{CLZ} + V_{ci} + V_s + V_d \tag{18}$$

where V is a function of the unknown DOF $\varepsilon_{t,avg}$.

In addition to the shear resistance expressed by Eq. (18), the shear force acting on the shear wall is also derived from the moment equilibrium of the entire wall as follows:

$$V_{eq} = \begin{bmatrix} E_s A_s \varepsilon_{t,avg} z \\ +N\left[h/2-(d-z)\right] \end{bmatrix} / a \tag{19}$$

$$z = \min\left[-0.6\frac{N}{f_c'bh}+0.9, 0.9\right]d \tag{20}$$

where $E_s \approx 200$ GPa is the modulus of elasticity of the reinforcement, N is the axial load on the wall (positive for compression), and z is the lever arm of the vertical forces in the base section. In shear calculations of members without axial load, z is typically estimated at $0.9d$. In this study, Eq. (20) is proposed to capture in an approximate manner the decrease of z under increasing axial compression. This expression is derived based on multiple classical flexural analyses of wall sections with various properties.

Finally, as the shear forces expressed by Eqs. (18) and (19) must be equal, this equilibrium condition is used to determine DOF $\varepsilon_{t,avg}$ and the shear strength of the wall.

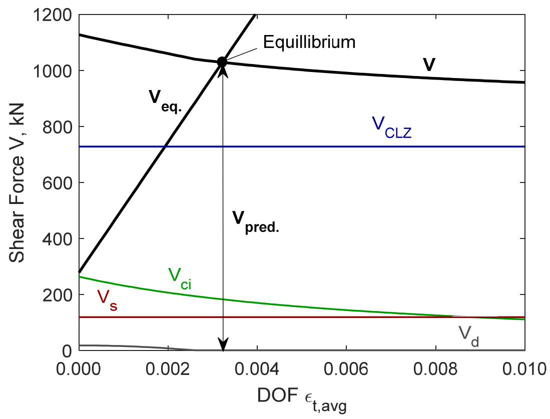

Fig. 4 Solution of the simplified 3PKT equations based on the equilibrium of the shear forces – specimen RF0 by (Franssen *et al*. 2021).

This is illustrated graphically in **Fig. 4**, where both V and V_{eq} are plotted as functions of $\varepsilon_{t,avg}$. The solution of the 3PKT equations lies at the intersection of the two curves, which is found by iterative calculations (e.g., the bisection method). The ordinate of the intersection point is the predicted shear strength of the wall V_{pred}.

Taking into account the simplifying assumptions of the proposed model, its applicability is limited to relatively short walls with a/h ratios ≤ 3.0 and normalized axial compression $n=N/f_c'bh \leq 0.4$. In addition, given the available test data that can be used for the validation of the model, the compressive strength of the concrete is limited in the range $20 \leq f_c' \leq 60$ MPa, which includes most practical cases. It is also noted that the model does not capture other failure modes such as sliding shear, out-of-plane instability, or detailing/lap splice failures.

4. Sample 3PKT calculations

To illustrate the calculations required by the proposed approach, it is applied to shear wall RF0 tested by (Franssen *et al*. 2021). The wall had a length h=1500 mm and an aspect ratio a/h=1.70. The total vertical reinforcement ratio was ρ_l=1.75% and the transverse reinforcement ratio was ρ_v=0.07%. The wall was subjected to an axial load N=1200 kN ($n=N/bhf_c'$=0.07) and failed under a shear force V_{exp}=1043 kN. All properties of the wall are provided in **Table 1**.

Figure 5(a) shows a photograph of the wall after failure and **Fig. 5(b)** shows the deformed shape at failure (scaled ×10) measured via digital image correlation (Langer 2019). The gray scale in **Fig. 5(b)** corresponds to the sum of the principal strains $|\varepsilon_1|+|\varepsilon_2|$ obtained from the measured displacement field. The critical diagonal crack and CLZ can be clearly identified in both figures. It can also be seen that the global deformation pattern of the wall is in agreement with the idealized kinematics in **Fig. 1(a)**.

Step-by-step calculations for the shear strength of

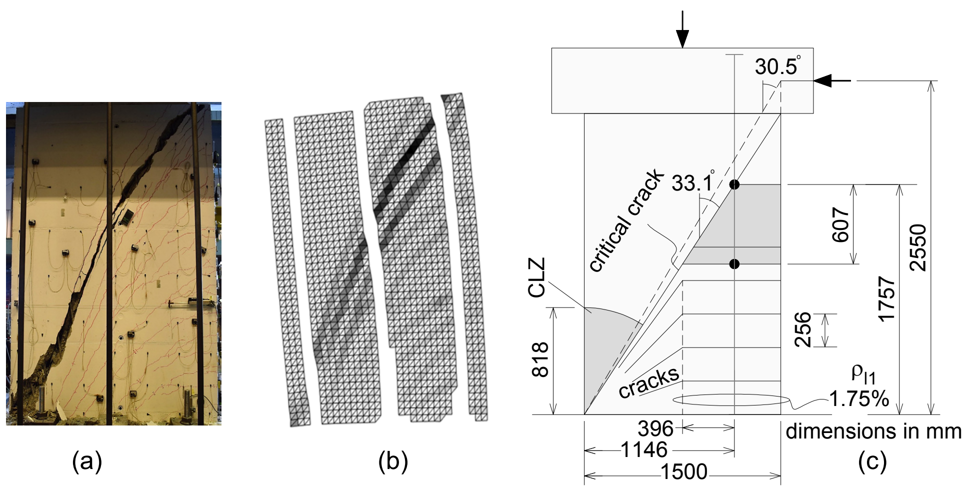

Fig. 5 3PKT modelling of test specimen RF0 by (Franssen *et al*. 2021): (a) Observed cracks and damage at failure; (b) Deformed shape (×10) obtained by digital image correlation (DIC) measurements at failure (Langer 2019); (c) Idealized crack pattern and critical loading zone.

wall RF0 are presented in the Appendix to the paper. The calculations begin with the geometry of the kinematic model, which is drawn to scale in **Fig. 5(c)**. For this wall, the critical crack extends along the diagonal of the test region at an angle $\alpha_1 \approx 33°$ as observed in the test. Using this geometry, the next step is to calculate DOFs Δ_c and Δ_{cx} associated with the CLZ: 4.65 mm and 0.59 mm, respectively. The shear carried in the CLZ is also calculated in this step: V_{CLZ}=727 kN. The other three shear mechanisms, as well as DOF $\varepsilon_{t,avg}$, are determined through iterative calculations by varying $\varepsilon_{t,avg}$ and checking the equilibrium condition $V=V_{eq}$. The relationships $V(\varepsilon_{t,avg})$ and $V_{eq}(\varepsilon_{t,avg})$ for specimen RF0 are plotted in **Fig. 4**.

It can be seen from **Fig. 4** that the final converged solution is reached at $\varepsilon_{t,avg}$=0.00330, which is slightly larger than the yield strain of the reinforcement. This is a conservative estimate that stems from the approximate nature of Eq. (20). It is also noted that some limited yielding was observed in the outer layers of the reinforcement in the test. The shear force at this strain is V_{pred}=1037 kN, corresponding to an experimental-to-predicted ratio V_{exp}/V_{pred}=1.01. The shear carried by the CLZ dominates the shear resistance with a contribution of 70.1% (727 kN). The shear carried by aggregate interlock is 191 kN or 18.4%. The shear carried by the light transverse reinforcement is 119 kN or 11.5%. Finally, the dowel action is predicted to have a negligible strength contribution due to the high longitudinal strain in the flexural reinforcement.

5. Validation dataset and comparisons with code equations

For the sake of a more thorough validation of the proposed simplified 3PKT approach, a dataset of 69 short shear walls with $a/h \leq 3.0$ were collected from past experimental studies (Franssen *et al.* 2021; Hirosawa 1975; Maier and Thürlimann 1985; Wiradinata 1985; Lefas e*t al.* 1990; Pilakoutas and Elnashai 1995; Lopes 2001; Oh *et al.* 2002; Greifenhagen and Lestuzzi 2005; Dazio *et al.* 2009; Bimschas 2010; Liu *et al.* 2010; Hannewald *et al.* 2013; Choun and Park 2015; Luna *et al.* 2015; Tran and Wallace 2015; Christidis *et al.* 2016; Yuniarsyah *et al.* 2017; Ji *et al.* 2018; Terzioglu *et al.* 2018; Xiong *et al.* 2018; Hosseini *et al.* 2019; Huang *et al.* 2020; Nie *et al.* 2020; Rong *et al.* 2020; Zhou *et al.* 2021; Wu *et al.* 2022) as shown in **Table 1**. This dataset features a wide range of test variables including different material and geometrical properties. The length of the walls h varies from 450 mm to 3050 mm, the a/h ratio from 0.3 to 3.0, the vertical reinforcement ratio ρ_l from 0.4% to 3.0%, the transverse reinforcement ratio ρ_v from 0 to 1.4%, the concrete compressive strength from 20.1 MPa to 57.5 MPa, and the normalized vertical force n from 0.1 in tension to 0.4 in compression. This dataset does not include failures reported as sliding-shear, out-of-plane instability, or failures due to poor detailing/lap splice deficiencies. The tests are divided into two subsets, i.e., shear failures (S) and flexural failures (F) according to the 3PKT shear strength predictions and flexural strength predictions. The minimum of these two predictions determines the governing failure mode and the predicted strength V_{pred} of each wall (reported in **Table 1**).

The main assumptions used for the flexural strength calculations are summarized in **Fig. 6**. The normal strains in the base section of the wall vary linearly along the section, starting from a strain of −0.0035 at the compressive edge. The distribution of the vertical reinforcement is simplified in two types of zones: end zones of length t_c (hidden columns) and a middle zone of length $l_m=h-2t_c$ (web of the wall). The bars in the end zones are lumped in the middle of length t_c, while those in the middle zone are smeared along length l_m. The compressive stresses in the concrete are approximated by using stress block factors according to Eurocode EC2 (CEN 2004), while the behavior of the reinforcement in tension and compression is simplified as elastic-perfectly-plastic. The equilibrium of the vertical forces is used to determine the position of the neutral axis, and the moment equilibrium to evaluate the lateral force on the wall at flexural failure.

Figure 7 and **Table 1** illustrate the accuracy of the flexural and shear strength predictions in terms of experimental-to-predicted ratios V_{exp}/V_{pred}. For the flexural strength of 40 wall specimens, the average V_{exp}/V_{pred} ratio is 1.05 and the coefficient of variation (COV) is 10.0%. For the shear strength of the remaining 29 specimens, the average ratio is 1.10 and the COV is 10.5%. These results show that (on average) the 3PKT is slightly conservative, and that the scatter of its predictions is similarly low as that of the flexural predictions. It is also noted with regards to **Fig. 7(a)** that the shear failure dominates at low a/h ratios, and the flexural failure governs in the range of $a/h \geq\approx 2.0$. Moreover, **Fig. 7(b)** shows that the 3PKT exhibits no apparent bias with respect to the shear reinforcement ratio ρ_v, which is varied widely from 0 to 1.40%. If the same calculations are performed with the original 3PKT, the average V_{exp}/V_{pred} ratio is slightly less conservative at 1.04, while the COV is slightly larger at 13.4%.

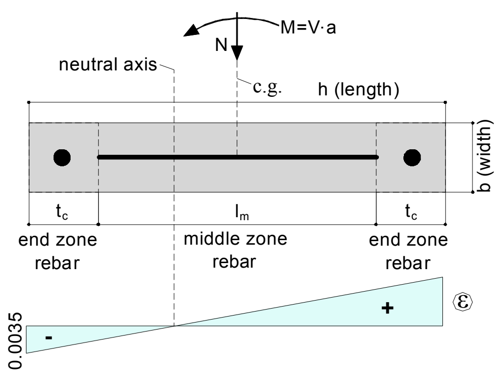

Fig. 6 Assumption for simplified flexural analysis of shear walls.

Table 1 Measured and predicted strength of shear walls by the simplified 3PKT and flexural analysis.

Specimen	Reference	a/h	b	h	t_c	d	d_1	a	a_{cl}	ρ_l	d_b	$\rho_{l,web}$	f_y	ρ_v	f_{yv}	f_c'	a_g	$n=N/f_c'bh$	V_{exp}	V_{pred}	V_{exp}/V_{pred}	Failure	V_{exp}/V_{ASCE}
		-	mm	mm	mm	mm	mm	mm	mm	%	mm	%	MPa	%	MPa	MPa	mm	-	kN	kN	-	-	-
73		1.00	160	1700	85	1419	1657	1700	1600	1.54	19	0.50	384	0.26	427	21.2	16	0.09	796	666	1.19	S	1.29
74	Hirosawa (1975)	1.00	160	1700	85	1419	1657	1700	1600	1.54	19	0.50	384	0.57	430	21.2	16	0.09	786	828	0.95	S	0.80
82		2.00	160	850	85	735	807	1700	1600	2.31	22	0.40	388	0.57	430	21.2	16	0.09	321	336	0.95	F	-
S9	Maier (1985)	1.12	100	1180	50	885	1154	1322	1200	0.99	8	0.99	560	0.00	0	29.2	16	0.08	342	272	1.26	S	2.15
S10		1.12	100	1180	200	1004	1154	1322	1200	2.91	16	1.00	513	0.98	496	31.0	16	0.07	670	648	1.03	S	1.23
Wall2	Wiradinata (1985)	0.33	100	2000	60	1585	1970	660	500	0.80	11.3	0.70	435	0.26	425	22.0	12	0.00	683	593	1.15	S	1.50
SW12		1.10	70	750	140	573	720	825	750	2.68	8	2.45	470	1.10	520	47.9	10	0.10	340	355	0.96	S	1.13
SW15	Lefas *et al.* (1990)	1.10	70	750	140	573	700	825	750	2.68	8	2.45	470	1.10	520	37.8	10	0.10	320	315	1.02	S	1.19
SW22		2.12	65	650	140	499	620	1378	1300	2.86	8	2.51	470	0.82	520	44.9	10	0.10	150	155	0.97	F	-
SW26		2.12	65	650	140	499	620	1378	1300	2.86	8	2.51	470	0.40	520	25.5	10	0.00	123	120	1.03	F	-
SW4		2.10	60	600	110	511	580	1260	1200	2.82	12	0.50	535	0.39	545	36.9	10	0.00	107	114	0.94	F	-
SW5		2.10	60	600	60	545	580	1260	1200	3.01	16	0.47	500	0.31	400	31.8	10	0.00	113	119	0.95	F	-
SW6	Pilakoutas and Elnashai (1995)	2.10	60	600	110	511	580	1260	1200	2.82	12	0.31	535	0.31	400	38.6	10	0.00	113	112	1.01	F	-
SW7		2.10	60	600	60	545	580	1260	1200	3.01	16	0.47	500	0.39	545	32.0	10	0.00	127	119	1.06	F	-
SW8		2.10	60	600	110	515	580	1260	1200	2.93	10	0.31	430	0.42	400	45.8	10	0.00	94	95	0.99	F	-
SW9		2.10	60	600	110	515	580	1260	1200	2.93	10	0.31	430	0.56	400	38.9	10	0.00	103	94	1.09	F	-
SW13		1.10	45	450	75	401.3	435	495	495	2.36	8	0.56	515	0.93	414	*44.0*	*10*	0.00	108	103	1.05	F	-
SW16	Lopes (2001)	1.10	45	450	75	401.3	435	495	495	2.11	8	0.00	527	1.40	414	*35.6*	*10*	0.00	80	88	0.92	F	-
SW17		1.10	45	450	75	401.3	435	495	495	2.11	8	0.00	527	0.80	414	*36.1*	*10*	0.00	84	88	0.95	F	-
SW18		1.10	45	450	75	401.3	435	495	495	2.73	12	0.00	533	0.80	414	*35.7*	*10*	0.00	100	103	0.97	S	1.03
WR-0		2.00	200	1500	150	1250	1450	3000	2000	0.67	13	0.36	449	0.31	342	27.6	19	0.10	394	391	1.01	F	-
WR-10	Oh *et al.* (2002)	2.00	200	1500	150	1250	1450	3000	2000	0.67	13	0.36	449	0.31	342	27.6	19	0.10	397	391	1.01	F	-
WR-200		2.00	200	1500	150	1250	1450	3000	2000	0.67	13	0.36	449	0.31	342	27.6	19	0.10	415	391	1.06	F	-
M3	Greifenhagen and Lestuzzi (2005)	0.77	80	900	40	786.5	880	690	565	0.39	6	0.32	504	0.26	745	*20.1*	*10*	0.10	176	163	1.08	F	-
WSH1		2.28	150	2000	175	1685	1975	4560	4030	0.54	10	0.30	562	0.25	584	45.0	*10*	0.05	336	333	1.01	F	-
WSH2		2.28	150	2000	175	1685	1975	4560	4030	0.54	10	0.30	542	0.25	485	40.5	*10*	0.06	359	334	1.08	F	-
WSH3	Dazio *et al.* (2009)	2.28	150	2000	230	1668	1970	4560	4030	0.82	12	0.54	587	0.25	489	39.2	*10*	0.06	454	445	1.02	F	-
WSH4		2.28	150	2000	230	1668	1970	4560	4030	0.82	12	0.54	550	0.25	519	40.9	*10*	0.06	443	435	1.02	F	-
WSH5		2.28	150	2000	230	1618	1975	4560	4030	0.39	8	0.27	523	0.25	519	38.3	*10*	0.13	439	404	1.09	F	-
WSH6		2.26	150	2000	230	1668	1975	4520	4030	0.82	12	0.54	550	0.25	519	45.6	*10*	0.11	597	564	1.06	F	-
VK1	Bimschas (2010)	2.20	350	1500	65	1190	1467	3300	3100	0.82	14	0.82	515	0.08	518	35.0	16	0.07	729	699	1.04	F	-
VK3		2.20	350	1500	65	1160	1467	3300	3100	1.23	14	1.23	515	0.08	518	34.0	16	0.07	879	879	1.00	F	-
N4T0	Liu *et al.* (2010)	1.86	100	700	100	609.8	675	1300	1200	2.49	14	0.44	414	0.44	414	38.9	10	0.15	297	261	1.14	F	-
N4T0		1.86	100	700	100	611.7	675	1300	1200	2.58	14	0.66	414	0.66	414	38.9	10	0.15	302	266	1.13	F	-
RW2		2.00	152.4	1219	180	1071	1191	2438	2362	2.84	19.1	0.61	477	0.61	443	48.6	9.5	0.07	730	708	1.03	F	-
RW3	Tran and Wallace (2015)	1.50	152.4	1219	180	1064	1191	1829	1753	1.31	12.7	0.33	472	0.33	516	48.8	9.5	0.08	589	558	1.06	F	-
RW4		1.50	152.4	1219	180	1057	1191	1829	1753	2.54	19.1	0.73	476	0.73	443	55.8	9.5	0.06	841	881	0.95	F	-
RW5		1.50	152.4	1219	180	1064	1191	1829	1753	2.46	19.1	0.61	476	0.61	443	57.5	9.5	0.02	665	728	0.91	F	-
VK6	Hannewald *et al.* (2013)	3.00	350	1500	65	1160	1467	4500	4300	1.23	14	1.23	521	0.08	528	44.4	16	0.06	666	682	0.98	F	-
VK7		2.20	350	1500	65	1160	1467	3300	3100	1.23	14	1.23	521	0.22	528	30.0	16	0.08	903	861	1.05	F	-

Table 1 (Continued from previous page).

Specimen	Reference	a/h	b	h	t_c	d	d_1	a	a_{cl}	ρ_l	d_b	$\rho_{l,web}$	f_y	ρ_v	f_{yv}	f_c'	a_g	$n=N/f_c'bh$	V_{exp}	V_{pred}	V_{exp}/V_{pred}	Failure	V_{exp}/V_{ASCE}
		-	mm	mm	mm	mm	mm	mm	mm	%	mm	%	MPa	%	MPa	MPa	mm	-	kN	kN	-	-	-
RC	Choun and Park (2015)	1.39	370	1220	100	915	1170	1700	1400	2.05	22	2.05	400	1.37	400	40.2	19	0.00	1323	1274	1.04	F	-
SW5	Luna *et al.* (2015)	0.33	203	3050	135	2290	2982	1007	854	1.00	12.7	1.00	462	1.00	462	29.7	20	0.00	2830	2361	1.20	S	1.01
SW6		0.33	203	3050	135	2290	2982	1007	854	0.67	12.7	0.67	462	0.67	462	26.2	20	0.00	2183	1953	1.12	S	0.83
SW9		0.54	203	3050	135	2290	2982	1647	1495	1.50	12.7	1.50	462	0.67	462	29.7	20	0.00	2820	2322	1.21	S	1.02
SW10		0.54	203	3050	135	2290	2982	1647	1495	1.50	12.7	1.50	462	0.33	462	31.7	20	0.00	2350	2256	1.04	S	1.29
W13	Christidis *et al.* (2016)	2.00	125	750	55	634.5	721	1500	1400	1.21	12	1.05	580	0.11	568	25.4	10	0.00	146	151	0.97	F	-
NSW2	Yuniarsyah *et al.* (2017)	1.33	120	1050	95	881.7	995	1400	1050	0.67	13	0.26	355	0.26	347	24.2	10	0.15	290	245	1.18	F	-
T2-S2	Terzioglu *et al.* (2018)	0.63	120	1500	250	1288	1460	950	750	1.40	16	0.67	455	0.67	481	25.8	*10*	0.00	666	628	1.06	S	0.88
T2-S3		0.63	120	1500	250	1288	1460	950	750	1.40	16	0.67	513	0.67	584	29.0	*10*	0.00	813	673	1.21	S	1.01
T4-S1		0.47	120	1500	90	1263	1460	700	500	1.19	14	0.67	547	0.67	584	34.8	*10*	0.00	874	757	1.15	S	0.99
T5-S1		1.13	120	1500	90	1380	1460	1700	1500	1.97	22	0.34	536	0.67	584	35.0	*10*	0.00	710	802	0.89	F	-
T6-S1		1.13	120	1500	90	1342	1460	1700	1500	2.19	22	0.67	541	0.67	584	22.6	*10*	0.00	735	752	0.98	S	1.03
T1-S2		0.63	120	1500	250	1343	1460	950	750	1.17	16	0.34	499	0.34	584	24.0	*10*	0.00	563	560	1.01	S	0.98
T1-N5-S1		0.63	120	1500	250	1343	1460	950	750	1.17	16	0.34	499	0.34	584	26.3	*10*	0.05	789	602	1.31	S	1.35
T1-N10-S1		0.63	120	1500	250	1343	1460	950	750	1.17	16	0.34	499	0.34	584	27.0	*10*	0.10	793	623	1.27	S	1.35
T1-S1		0.63	120	1500	90	1343	1460	950	750	1.17	16	0.34	450	0.34	481	23.7	*10*	0.00	635	553	1.15	S	1.25
SW6	Ji *et al.* (2018)	1.10	180	1500	280	1311	1450	1650	1350	2.54	22	0.58	477	0.37	480	*42.1*	*10*	0.00	1225	1111	1.10	S	1.33
SW0	Xiong *et al.* (2018)	1.50	180	1440	200	1239	1395	2160	2020	2.09	26	0.28	454	0.28	417	*32.3*	*10*	0.15	965	749	1.29	S	1.44
RCSW1	Hosseini *et al.* (2019)	0.90	150	1600	300	1342	1560	1435	1380	0.73	12	0.27	430	0.34	497	31.0	13	0.00	503	424	1.19	F	-
T00	Nie *et al.* (2020)	1.06	150	1700	250	1529	1650	1800	1500	2.47	16	0.38	443	0.38	402	49.8	10	0.00	1430	1203	1.19	S	1.71
T30		1.06	150	1700	250	1529	1650	1800	1500	2.47	16	0.38	443	0.38	402	49.8	10	-0.06	1127	895	1.26	F	-
T40		1.06	150	1700	250	1529	1650	1800	1500	2.47	16	0.38	443	0.38	402	49.8	10	-0.08	1049	792	1.32	F	-
T50		1.06	150	1700	250	1529	1650	1800	1500	2.47	16	0.38	443	0.38	402	49.8	10	-0.10	952	683	1.39	F	-
SW9	Rong *et al.* (2020)	2.14	100	700	100	603.6	678	1500	1400	1.62	12	0.38	381	0.28	270	*44.0*	15	0.19	213	222	0.96	S	1.61
H1.0-R	Huang *et al.* (2020)	1.20	100	1000	100	750	950	1200	1000	1.57	10	1.57	413	0.38	390	*24.6*	*10*	0.10	266	279	0.95	S	0.98
SSW-1	Zhou *et al.* (2021)	1.14	100	700	100	624.8	684	800	700	1.62	12	0.38	341	0.28	305	20.6	*10*	0.20	162	176	0.92	S	1.16
RF0	Franssen *et al.* (2021)	1.70	230	1500	75	1146	1461	2550	2300	1.75	16	1.75	522	0.07	578	52.3	16	0.07	1043	1032	1.01	S	1.38
A1	Wu *et al.* (2022)	1.16	200	2500	400	2033	2465	2900	2750	0.75	14	0.39	413	0.39	415	*40.1*	*10*	0.30	1678	1636	1.03	S	1.04
B1		1.16	200	2500	400	2033	2465	2900	2750	0.75	14	0.39	413	0.39	415	*40.1*	*10*	0.40	1814	1657	1.09	S	1.13

Notations:
a/h = shear-span-to-length-ratio; b = width of wall cross-section; h = length of wall section; d = effective length of section; d_1 = distance from compressive edge of section to furthest tension longitudinal bar; a = wall height subjected to shear; a_{cl} = clear height of wall; ρ_l = ratio of total longitudinal reinforcement; d_b = diameter of main flexural reinforcement; $\rho_{l,web}$ = ratio of longitudinal web reinforcement;
f_y = yield strength of longitudinal reinforcement; ρ_v = ratio of transverse reinforcement; f_{yv} = yield strength of transverse reinforcement; f_c' = compressive cylinder strength; a_g = concrete maximum aggregate size; $n = N/bhf_c'$ = vertical axial force ratio; V_{exp} = experiment shear strength, V_{pred} = predicted lateral strength which is smaller of (3PKT shear strength, flexural strength); Failure = failure mode (F: flexural, S: shear failure).
Notes:
Italic values in the table are assumed or estimated due to missing reported data from the experiments.
*The failure modes (F or S) are based on the predicted strength values by the 3PKT and flexural analysis.

To further put these results in context, the 3PKT approach is compared to the shear provisions of the ASCE 41-13 code (ASCE 2014) – see **Fig. 8** and **Table 1**. The code uses the following semi-empirical equation for the shear strength of short walls:

$$V_{ASCE} = (\alpha_c\sqrt{f_c'} + \rho_v f_y v)bh \leq 0.83\sqrt{f_c'}\cdot bh \text{ (MPa)} \quad (21)$$

where α_c=0.17 for a_{cl}/h≥2.0 and 0.25 for a_{cl}/h≤1.5, with a linear transition for intermediate values of a_{cl}/h. Eq. (21) implies that the transverse reinforcement is taken into account along a 45° crack (see second term), and that the concrete shear components are lumped in the first term of the equation. The positive effect of the transverse reinforcement is limited by the upper bound imposed on the shear strength.

As evident from **Fig. 8**, the ASCE 41-13 code (ASCE 2014) is more conservative than the 3PKT approach, resulting in an average shear strength experimental-to-predicted ratio of 1.21. The code also results in a significantly larger scatter: a COV of 23.8%. The scatter appears to be linked mainly to the effect of the transverse reinforcement. As evident from **Fig. 8(b)**, the code tends to be very conservative for walls with small reinforcement ratios ρ_v≤≈0.3%. For instance, the V_{exp}/V_{ASCE} ratio for wall RF0 with ρ_v=0.07% is 1.38, compared to 1.01 obtained with the 3PKT. The most conservative code prediction is obtained for specimen S9 (Maier and Thürlimann 1985) without transverse reinforcement: V_{exp}/V_{ASCE}=2.15 versus V_{exp}/V_{pred}=1.26 for the 3PKT. These results show that, while the 3PKT requires more calculations, it can significantly improve the shear strength predictions. This can be particularly important in the assessment of existing lightly reinforced structures, where overly conservative predictions can result in costly and disruptive strengthening interventions. It is evident that the ASCE code significantly underestimates the shear contribution of the concrete.

A semi-empirical equation [see Eq. (22)] for shear strength is also provided by the Japanese seismic code (AIJ 2001). The equation has a more limited application as the aspect ratio of the wall needs to be between 1 and 3. Within this range, there are 17 specimens in the database that were shear critical. For this limited set, the AIJ standard produces more conservative results than the ASCE code with an average V_{exp}/V_{AIJ} ratio of 1.36 and a COV of 18.1%, as shown in **Fig. 9**.

$$V_{AIJ} = \left[\left(\frac{0.053\rho_l^{0.023}(18+f_c')}{\frac{a}{h}+0.12} + 0.85\sqrt{\rho_v f_{yv}} + 0.1(nf_c')\right)\right]0.8bh \text{ (MPa)} \quad (22)$$

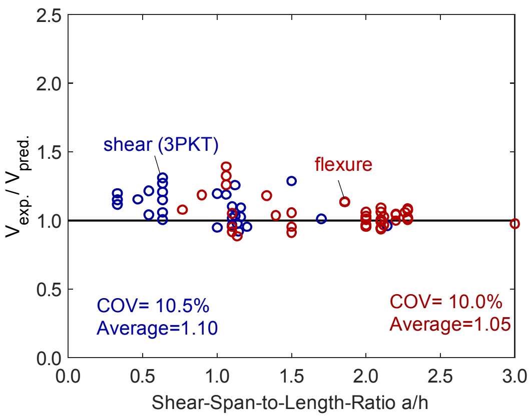

(a) Effect of shear-span-to-length ratio *a/h*

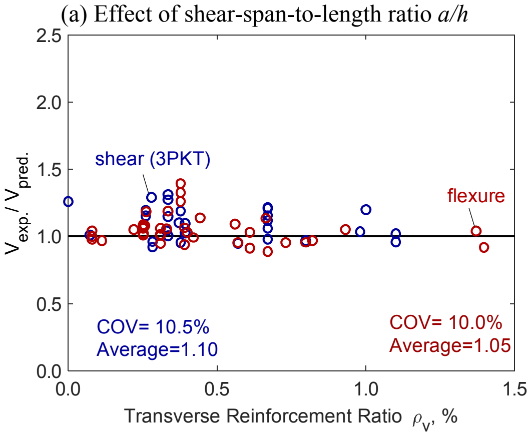

(b) Effect of transverse reinforcement ratio ρ_v

Fig. 7 3PKT shear strength predictions and flexural strength predictions for a database of 69 shear wall tests.

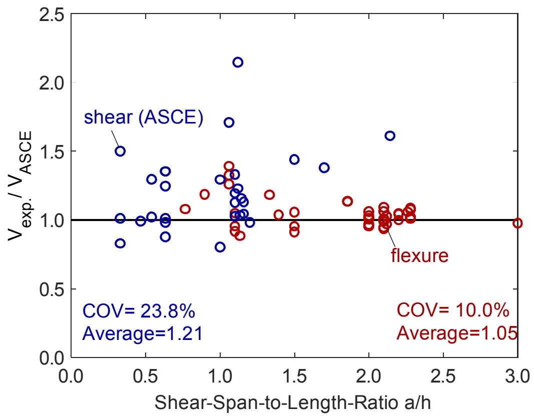

(a) Effect of shear-span-to-length ratio *a/h*

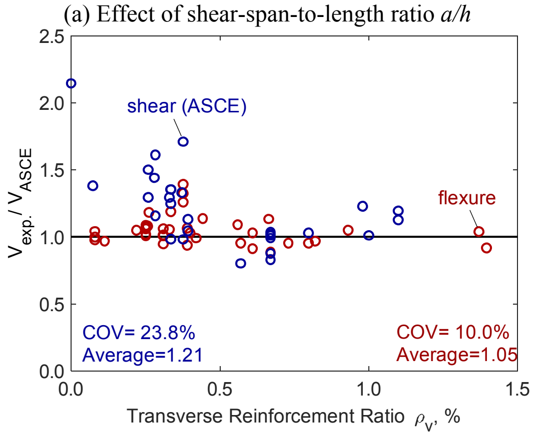

(b) Effect of transverse reinforcement ratio ρ_v

Fig. 8 ASCE (2014) shear strength and flexural strength predictions for a database of 69 shear wall tests.

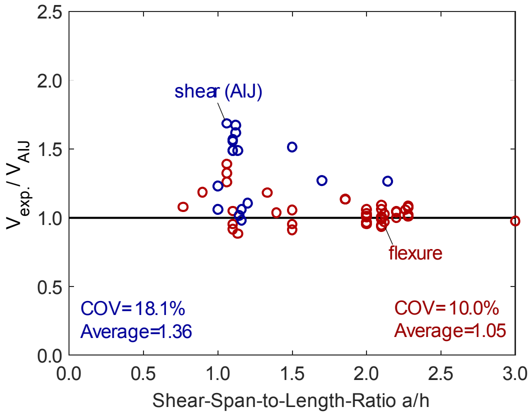

(a) Effect of shear-span-to-length ratio *a/h*

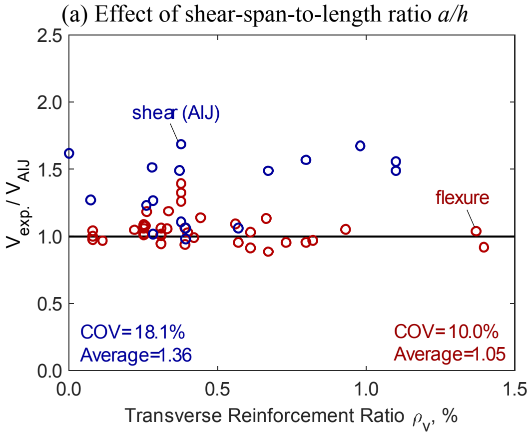

(b) Effect of transverse reinforcement ratio ρ_v

Fig. 9 AIJ (2001) shear strength and flexural strength predictions for a database of 69 shear wall tests.

6. Effect of wall properties on the shear strength

In addition to the overall validation of the 3PKT approach with 29 wall specimens, it is also of interest to study the effect of different wall properties on the ultimate shear behavior of such members. In the following, individual wall series are selected that feature a single test variable, and their shear strength and shear mechanisms are predicted with the 3PKT. As there can be slight variations in material properties between test specimen, the predictions are performed with averaged properties within each test series.

6.1 Effect of reinforcement ratio

A test series reported by Luna *et al*. (2015) is suitable to study the effect of the reinforcement ratio on the shear strength (**Table 1**). The specimens were reinforced with uniform orthogonal reinforcement without hidden end columns. Specimens SW5 and SW6 had the same sectional dimensions (b=203 mm and h=3050 mm) with an aspect ratio a/h=0.33, and differed mainly in the amount of vertical and horizontal reinforcement: ρ_l=ρ_v=1.0% for SW5 and ρ_l=ρ_v=0.67% for SW6.

Figure 10 compares the measured shear strengths of specimens SW5 and SW6 to the 3PKT predictions, both normalized by the area of the section and by f_c'. As evident from the plot, an increase of ρ_l and ρ_v of 50% leads to an increase in measured shear strength of around 21%, and an increase of predicted strength of around 13%. The increase is predicted to result mainly from shear components V_s and V_{ci}, which are plotted in the figure together with components V_{CLZ} and V_d. As can be expected, component V_s increases linearly with the amount of transverse reinforcement [Eq. (16)]. At the same time, the increase of aggregate interlock contribution is explained with the width of the critical crack at failure. The crack width is plotted on the right axis of **Fig. 10** and decreases with increasing ρ_l and ρ_v due to the crack control provided by the reinforcement, and in particular by the vertical reinforcement which is elastic. The smaller is the crack width, the stronger is the aggregate interlock mechanism as expressed by Eq. (15).

A similar analysis is performed for specimens SW9 and SW10 (Luna *et al*. 2015), which had an aspect ratio of 0.54 and differed mainly in terms of the transverse reinforcement ratio: ρ_v=0.67% for SW9 and 0.33% for SW10. The results are shown in **Fig. 11** in the same format as **Fig. 10**. The plot shows that when ρ_v is dou-

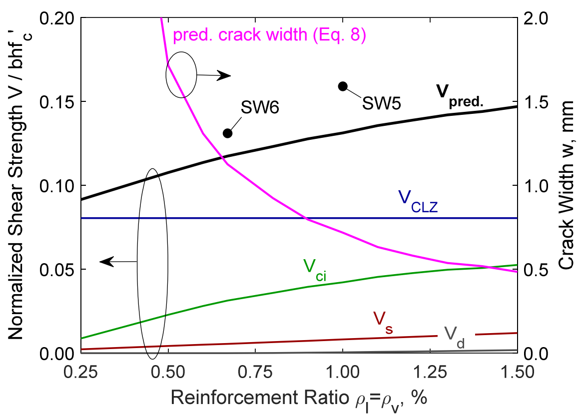

Fig. 10 Effect of amount of vertical and transverse reinforcement on the shear strength of short walls - Tests by Luna *et al*. (2015) with average properties *a/h*=0.33, *h*=3050 mm, f_c'=28 MPa, and *n*=0.

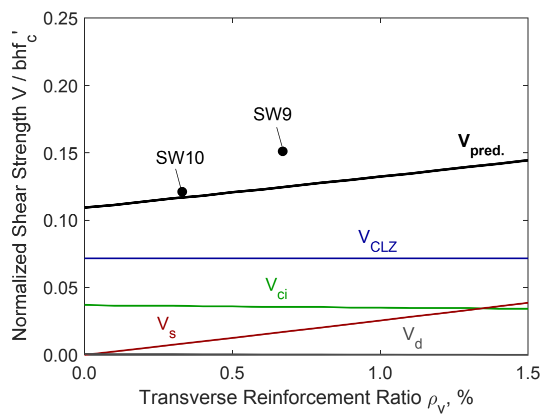

Fig. 11 Effect of amount of transverse reinforcement on the shear strength of short walls walls - Tests by Luna *et al*. (2015) with average properties *a/h*= 0.54, *h*=3050 mm, f_c'=30.7 MPa, ρ_l=1.5%, and *n*=0.

bled, the measured shear strength increases by around 25% and the 3PKT prediction by 7%. As discussed earlier, increasing ρ_v results in a linearly increasing shear contribution of the transverse reinforcement V_s. On the other hand, because the transverse reinforcement yields before failure, ρ_v does not contribute significantly to the control of the critical diagonal crack (no crack control by ρ_v is assumed in the 3PKT), and therefore the aggregate interlock contribution V_{ci} is predicted to remain nearly constant.

It is noted that the ASCE code produced better shear strength predictions for specimens SW5 and SW9 than the 3PKT approach (**Table 1**). The code predictions for both specimens are governed by the upper limit on the shear strength imposed in Eq. (21). This limit implies that the failure occurred with inclined crushing/sliding of the wall, which is consistent with the test observations (Luna 2016). However, when the transverse reinforcement is reduced in the companion specimens SW6 and SW10, and when yielding of the reinforcement begins to govern the response (particularly for SW10), the code predictions become inconsistent (i.e., either unconservative or conservative, respectively).

It is also noted that the crushing/sliding failures observed in the shortest specimens SW5 and SW6 (a/h=0.33) are not fully captured by the 3PKT. More specifically, while walls SW5 and SW6 failed along nearly horizontal planes, the 3PKT assumes a diagonal failure crack. Nevertheless, as the diagonal crack is very flat, the 3PKT shear strength predictions remain reasonably close to the measured values.

6.2 Effect of concrete strength

To study the effect of the compressive strength of the concrete f_c', test specimens SW9 and SW10 by Lefas *et al*. (1990) are selected from the test database. The specimens had the same dimensions and an aspect ratio of 1.10, with the measured values of f_c' varying from 47.9 MPa for SW9 to 37.8 MPa for SW10. **Figure 12** shows that when the concrete strength was increased by 27%, the measured shear strength of the walls increased by around 3%, and the 3PKT prediction by 9%. Naturally, this strength increase is explained with the enhancement of the concrete shear mechanisms, i.e., the inclined compression in the CLZ (V_{CLZ}) and the aggregate interlock along the critical crack (V_{ci}).

6.3 Effect of axial load

Specimens A1 and B1 by (Wu *et al*. 2022) are used to study the effect of axial compression on the shear strength of short walls. The aspect ratio of the specimens was 1.16 and the normalized axial load $n=N/bhf_c'$ was varied from 0.3 in A1 to 0.4 in B1. **Figure 13** shows that the 33% increase of axial compression resulted in a slight increase in shear strength according to both the tests (8%) and the 3PKT approach (2%). It can also be seen that the model predicts that the axial load has a small influence on the shear strength across the entire range of analyzed n values from 0 to 0.4. The only shear component that is predicted to increase slightly with n is V_{ci}. The higher is the axial compres-

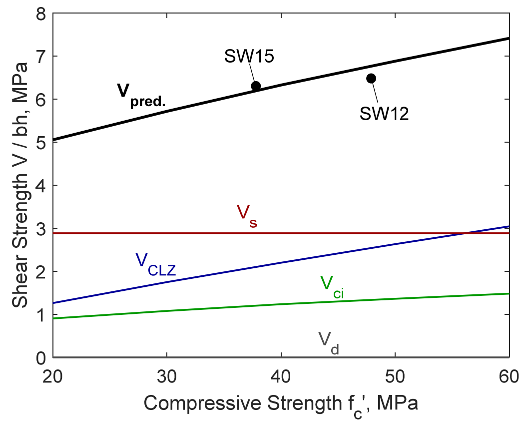

Fig. 12 Effect of compressive strength of concrete on the shear strength of short walls - Tests by Lefas *et al.* (1990) with average properties a/h=1.10, h=750 mm, ρ_l=2.7%, ρ_v=1.1%, and n=0.1.

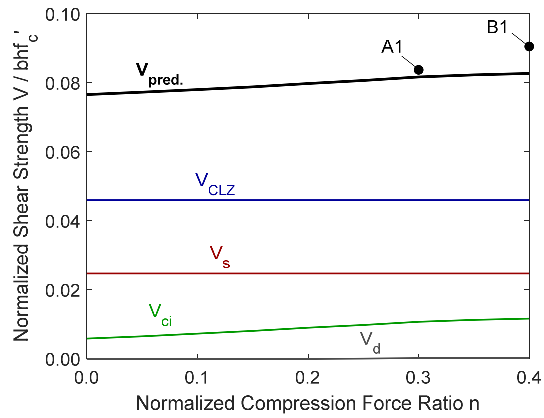

Fig. 13 Effect of axial compression on the shear strength of short walls - Tests Wu *et al.* (2022) with average properties a/h=1.16, h=2500 mm, f_c'=40.1 MPa, ρ_l=0.75%, and ρ_v=0.39%.

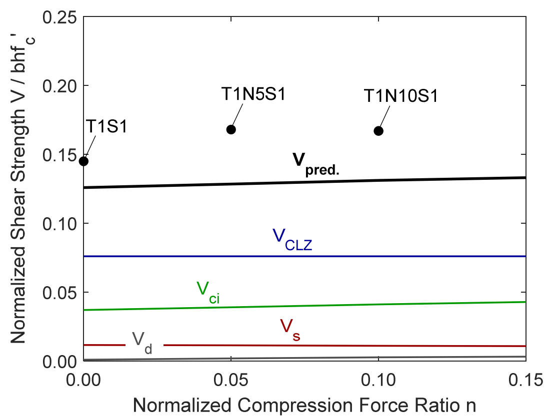

Fig. 14 Effect of axial compression on the shear strength of short walls - Tests by Terzioglu *et al.* (2018) with average properties a/h=0.63, h=1500 mm, f_c'=25.7 MPa, ρ_l=1.17%, and ρ_v=0.34%.

sion on the wall, the smaller is the strain in the flexural tensile reinforcement and the narrower is the critical crack, thus resulting in a more effective interlocking of the crack surfaces.

A different range of axial load values was tested by Terzioglu *et al*. (2018): specimens T1-S1, T1-S1-N5 and T1-S1-N10 had n values of 0, 0.05 and 0.1, respectively. Compared to specimens A1 and B1, these walls featured a smaller section (h=1500 mm vs. 2500 mm), a smaller aspect ratio (a/h=0.63 vs. 1.16), similar amounts of web reinforcement ratio (≈0.35% in both directions), and larger total vertical reinforcement ratio (ρ_l=1.17% vs. 0.75%). Nevertheless, the trend illustrated in **Fig. 14** is similar to that in **Fig. 13**, i.e., a slight increase of shear strength with increasing axial compression according to both the tests and predictions, even though the predictions in this case are rather conservative. This trend is distinctly different from those observed in slender members, where the axial load has been shown to enhance the shear strength (Collins *et al.* 2016) significantly.

6.4 Effect of aspect ratio *a*/*h*

The effect of wall slenderness is studied with the help of two walls from different test series: specimen SSW-1 (Zhou *et al*. 2021) and SW9 by (Rong *et al*. 2020) (**Table 1**). The walls had a length h=700 mm, total vertical reinforcement ρ_l=1.62%, vertical and horizontal web reinforcement $\rho_{l,web}$=0.38% and ρ_v=0.28%, respectively, and a normalized axial load n≈0.20. The main differences between the walls were the concrete strength f_c' of 20.6 MPa for SSW-1 and 44.0 MPa for SW9, as well as the aspect ratio a/h of 1.14 and 2.14, respectively.

Due to the significant difference in concrete strength, the 3PKT calculations are performed with both values of f_c' for a wide range of a/h ratios – see **Fig. 15**. The shear forces are normalized by $f_c'^{0.7}$ (MPa) in order to minimize the influence of the compressive strength on the concrete shear V_{CLZ} and V_{ci}. The obtained shear strength experimental-to-predicted ratios for SSW-1 and SW9 are 0.92 and 0.96, receptively. **Figure 15** illustrates clearly the transition from short to slender walls predicted by the 3PKT and consistent with the experimental points. In very short (or squat) walls, the shear strength is high and decreases rapidly with increasing *a/h*. Following this rapid decrease, the strength gradually approaches a nearly constant value in slender members with a/h≥≈2.5.

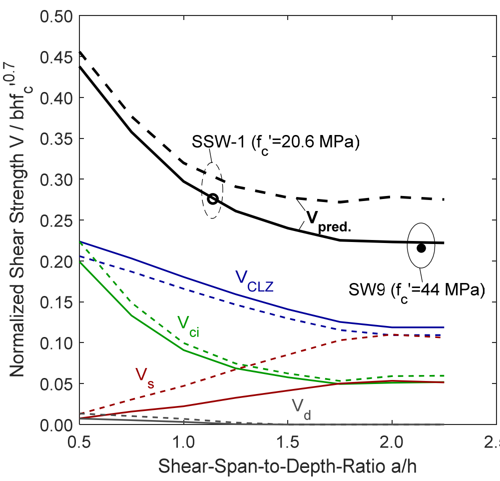

Fig. 15 Effect of aspect ratio on the shear strength of short walls - Tests by Zhou *et al*. (2021) and Rong *et al*. (2020) with properties h=1500 mm, f_c'=20.6 MPa and 44.0 MPa, respectively, ρ_l=1.62%, ρ_v=0.28%, and n=0.2.

This trend is underlined by shear contributions V_{CLZ}, V_{ci} and V_s. As a/h increases, the angle of the critical crack decreases, leading to a higher contribution of the transverse reinforcement V_s (more bars cross the crack). On the other hand, the CLZ becomes slenderer, which results in a reduction of its strength V_{CLZ} and an increase of its deformation Δ_c. In turn, as Δ_c increases, so does the width of the critical crack, leading to lower aggregate interlock contribution (V_{ci}). In total, the reduction of concrete contributions V_{CLZ} and V_{ci} is more rapid than the increase of reinforcement contribution V_s, thus resulting in a decreasing shear strength with increasing aspect ratio *a/h*. In slender walls, the strength becomes nearly constant as the angle of the critical crack ceases to decrease (α_1 is limited to a minimum of 30° in the 3PKT).

It should be noted that walls SSW-1 and SW9 confirm the observation made with regards to **Fig. 8(b)**. Even though the transverse reinforcement in these walls was larger than the minimum ratio of 0.25% typically required by designed codes (ACI 2014), their shear strength is significantly underestimated by the ASCE 41-13 shear provisions. The obtained V_{exp}/V_{pred} ratios are 1.16 for the shorter wall and 1.61 for the slenderer specimen. It is worth noting that the crack angle in the shorter specimen α_1 is approximately 45° as $h=a_{cl}$, and thus equal to the assumed angle in the ASCE 41-13 equation. Therefore, the shear contribution of the transverse reinforcement is well predicted by the equation. This shows that the ASCE code significantly underestimates the shear carried by the concrete.

6.5 Size effect

It is well known that the shear carried by the concrete can exhibit size effect, particularly for members with less-than-minimum transverse reinforcement. Size effect has been studied extensively for beams and slabs without stirrups, where a significant decrease of shear stress at failure occurs as the size of the member increases (Collins and Kuchma 1999). It has also been shown that a certain minimum amount of stirrups can eliminate this effect (Collins and Kuchma 1999). However, because shear walls always feature web reinforcement even in older existing structures, less effort has been devoted to size effect studies of such members. This is evidenced by the test database, which does not include test series of geometrically similar walls with variable dimensions. Nevertheless, it is of interest to use the 3PKT method to

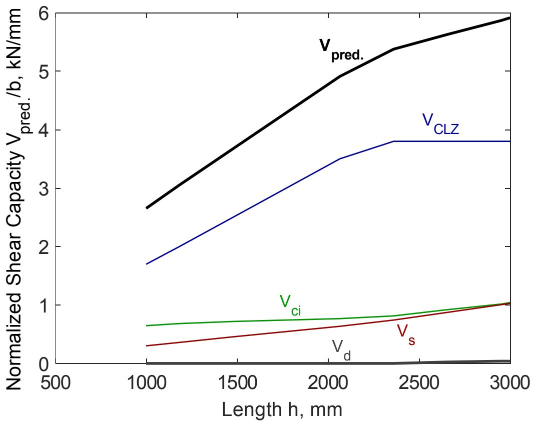

Fig. 16 Effect of members' size on the shear strength shear walls (wall properties: a/h=1.12; b=0.085h; d=0.75h; f_c'=29.2 MPa; ρ_l=1%; ρ_v=0.1%; a_g=16 mm; f_y=f_{yv}=560 MPa).

simulate the size effect in shear walls with small amounts of transverse reinforcement.

Figure 16 shows how the normalized shear strength V_{pred}/b varies with increasing wall dimensions. The simulations are performed on the basis of test specimen S9 (Maier and Thürlimann 1985) with a/h=1.12. All wall dimensions are scaled proportionally (see figure caption) up to an h of 3000 mm, except for the maximum size of the coarse aggregates which is kept constant. In addition, light transverse reinforcement with a ratio ρ_v=0.10% is added to the walls to represent realistic cases of existing structures (specimen S9 had no web reinforcement). It can be seen from **Fig. 16** that the shear strength does not increase proportionally with the wall length, and therefore the 3PKT predicts size effect. Up to h of approximately 2000 mm, the size effect is mostly caused by the aggregate interlock shear contribution V_{ci}. The larger is the wall, the wider is the critical diagonal crack, and therefore the smaller is the predicted aggregate interlock shear stress [Eq. (15)]. For larger walls, shear component V_{CLZ} also exhibits size effect, determined by the upper limit on the size of the CLZ imposed in Eq. (7). As mentioned earlier, this limit was proposed based on comparisons with limited data from large wall specimens (Mihaylov *et al*. 2016). However, while the upper limit can be devoted to localization of compressive deformations in the toe of the wall, it can be seen as a conservative approximation of a more complex nonlinear trend. Therefore, future experimental research is needed to understand better the localization effects in large lightly-reinforced walls.

7. Range of applicability

In summary, the 3PKT approach was developed for shear-dominated walls where the failure occurs along critical diagonal cracks. Considering the assumptions made in the derivation of the 3PKT, as well as the limits imposed by the validation database, the following range of applicability of the model should be respected:

a) Shear-span-to-length-ratio $a/h \leq 3$;
b) Rectangular sections;
c) Transverse reinforcement ratio $\rho_v \leq 0.6\%$;
d) Normalized compression ratio $n=(N/f_c'bh) \leq 0.4$.

Failures modes associated with sliding shear, out-of-plane instability, or inadequate detailing/lap splices need to be modelled separately. Further experimental and analytical research is needed to study the size effect in shear of large lightly-reinforced shear walls.

8. Conclusions

This paper presented a simplified three-parameter kinematic theory (3PKT) approach for the shear strength of reinforced concrete walls with aspect ratios ≤3.0. The original 3PKT for complete nonlinear analysis was simplified by estimating two of the three DOFs of the model at peak load, as well as by using simpler expressions for the mechanisms of shear resistance. The proposed model aimed to capture shear failures along diagonal cracks, and it is not applicable to other failure modes such as sliding shear, out-of-plane instability, or detailing/ lap splice failures.

The model was validated with a database of 29 shear critical test specimens, and the results were compared to those from the ASCE (2014) and AIJ (2001) shear provisions. It was found that the code provisions provide conservative and scattered shear strength predictions. The average experimental-to-predicted ratios produced by the two codes are respectively 1.21 and 1.36, and the COVs are 23.8% and 18.1%. In comparison, while the 3PKT requires more calculations, it reduces the average value to 1.10 and the COV to only 10.5%, achieving a similar accuracy to that of flexural strength calculations. The 3PKT was also shown to adequately capture the effect of key test variables on the shear strength of walls, including the amounts of flexural and shear reinforcement, concrete strength, level of axial load and aspect ratio of the wall.

Of particular importance in practice is the ratio of shear reinforcement which can vary widely in existing structures. Most importantly, existing structures can feature ratios that are smaller than the minimum values required by modern design codes (e.g., 0.25%). It was shown that the ASCE code is particularly conservative for such walls (up to 100% strength underestimation), and thus can result in costly and disruptive strengthening interventions. In contrast, the 3PKT maintains the same accuracy across the whole range of reinforcement ratios featured in the wall database, and therefore can be used as a reliable tool for shear assessment.

Notations

A_s = one-half of total area of total longitudinal reinforcement
A_v = area of transverse reinforcement resisting shear
a = wall height subjected to shear
a_{cl} = clear height of the wall

a_g = concrete maximum aggregate size
b = width of wall cross-section
d = effective length of section
d_1 = distance from compressive edge of section to furthest tension longitudinal bar
d_b = diameter of main flexural reinforcement
F_{CLZ} = compression force in the concrete of CLZ
$f_{c,CLZ}$ = average compressive strength in CLZ
f_y = yield strength of longitudinal reinforcement
f_{yv} = yield strength of transverse reinforcement
f_u = strength of longitudinal reinforcement
f_{uv} = strength of transverse reinforcement
f_v = stress in transverse reinforcement
h = length of wall section
l_{b1e} = characteristic length of CLZ
l_t = cracked length along longitudinal reinforcement
l_k = length of transition zone between fan and rigid block
l_0 = portion of l_k below the critical diagonal crack
M = bending moment at the base of the wall
N = axial load
n_b = number of bars corresponding to A_s
n_{cr} = number of major diagonal cracks
s_{cr} = crack spacing in effective tension zone
V = shear force and lateral load
V_{max} = peak shear force and peak lateral resistance
V_{ci} = aggregate interlock shear resistance
V_s = transverse reinforcement shear resistance
V_d = dowels shear resistance
w = crack width
Δ_{ci} = crack slip
α = angle of wall diagonal with respect to the vertical axis
α_1 = angle of critical crack
α_Δ = angle of displacement at CLZ
α_F = angle of force F_{CLZ}
Δ = applied lateral displacement
Δ_c = horizontal displacement at CLZ
Δ_{cx} = vertical displacement at CLZ
ε_{CLZ} = average strain in CLZ
$\varepsilon_{t,avg}$ = average strain along longitudinal tension reinforcement
ε_y = yield strain of longitudinal reinforcement
ε_u = breaking strain of longitudinal reinforcement
ε_v = strain in transverse reinforcement
ρ_l = ratio of total longitudinal reinforcement
$\rho_{l,w}$ = ratio of longitudinal web reinforcement
ρ_{l1} = reinforcement ratio in effective tension zone
ρ_v = ratio of transverse reinforcement

References

ACI, (2014). "*Building code requirements for structural concrete and commentary* (ACI-318-11)." Farmington Hills, Michigan: American Concrete Institute.

AIJ, (2001). "*Seismic evaluation criteria and retrofit design guidelines for existing reinforced concrete buildings, and commentary*." Tokyo: Architectural Institute of Japan. (in Japanese)

ASCE, (2014). "*Seismic evaluation and retrofit of existing buildings* (ASCE code 41-13)." Reston, Virginia: American Society of Civil Engineers.

Bažant, Z. P. and Oh, B. H., (1985). "Microplane model for progressive fracture of concrete and rock." *Journal of Engineering Mechanics*, 111(4), 559-82.

Beyer, K., Dazio, A. and Priestley, N., (2011). "Shear deformations of slender reinforced concrete walls under seismic loading." *ACI Structural Journal*, 108, 167-77.

Bimschas, M., (2010). "*Displacement based seismic assessment of existing bridges in regions of moderate seismicity*." Thesis (Doctoral). Swiss Federal Institute of Technology (ETH) Zürich.

Biskinis, D. and Fardis, M. N., (2010). "Flexure-controlled ultimate deformations of members with continuous or lap-spliced bars." *Structural Concrete*, 11(2), 93-108.

CEN, (2004). "*Design of concrete structures* (Eurocode EC2)." Brussels: European Committee for Standardization.

CEN, (2005). "*Design of structures for earthquake resistance - Part 3: Assessment and retrofitting of buildings* (Eurocode EC8)." Brussels: European Committee for Standardization.

Choun, Y. S. and Park, J., (2015). "Evaluation of seismic shear capacity of prestressed concrete containment vessels with fiber reinforcement." *Nuclear Engineering and Technology*, 47(6), 756-65.

Christidis, K. I., Vougioukas, E. and Trezos, K. G., (2016). "Strengthening of non-conforming RC shear walls using different steel configurations." *Engineering Structures*, 124, 258-68.

Collins, M. P., Xie, L., Mihaylov, B. I. and Bentz, E. C., (2016). "Shear response of prestressed thin-webbed continuous girders." *ACI Structural Journal*, 113(3), 447-457.

Collins, M. P. and Kuchma, D., (1999). "How safe are our large, lightly reinforced concrete beams, slabs, and footings?" *Structural Journal*, 96(4), 482-490.

Dazio, A., Beyer, K. and Bachmann, H., (2009). "Quasi-static cyclic tests and plastic hinge analysis of RC structural walls." *Engineering Structures*, 31(7), 1556-71.

Franssen, R., Courard, L. and Mihaylov, B. I., (2021). "Shear behavior of concrete walls retrofitted with ultra-high-performance fiber-reinforced concrete jackets." *ACI Structural Journal*, 118(5), 149-160.

Fu, L., Nakamura, H., Chi, S., Yamamoto, Y. and Miura, T., (2021). "Numerical evaluation of shear strength degradation mechanism dependent on the size increase of RC deep beams with height up to 1.5 meter by using 3-D rigid-body-spring-method." *Journal of Advanced Concrete Technology*, 19(12), 1245-1263.

Greifenhagen, C. and Lestuzzi, P., (2005). "Static cyclic tests on lightly reinforced concrete shear walls." *Engineering Structures*, 27(11), 1703-12.

Hannewald, P., Bimschas, M. and Dazio A., (2013).

"*Quasi-static cyclic tests on RC bridge piers with detailing deficiencies* (IBK Report No. 352)." Zürich: Institut für Baustatik und Konstruktion der ETH Zürich.

Hirosawa, M., (1975). "Past experimental results on reinforced concrete shear walls and analysis on them." *Kenchiku Kenkyu Shiryo*, 6, 33-4. (in Japanese)

Hosseini, S. A., Kheyroddin, A. and Mastali, M., (2019). "An experimental investigation into the impacts of eccentric openings on the in-plane behavior of squat RC shear walls." *Engineering Structures*, 197, 109410.

Huang, Z., Shen, J., Lin, H., Song, X. and Yao, Y., (2020). "Shear behavior of concrete shear walls with CFRP grids under lateral cyclic loading." *Engineering Structures*, 211, 10422.

Ji, X., Cheng, X. and Xu, M., (2018). "Coupled axial tension-shear behavior of reinforced concrete walls." *Engineering Structures*, 167, 132-42.

Kagermanov, A. and Ceresa, P., (2016). "Physically based cyclic tensile model for RC membrane elements." *Journal of Structural Engineering*, 142(12), 04016118.

Langer, M., (2019). "*Evaluation of the load-bearing mechanisms in coupling beams and shear walls based on DIC measurements*." Thesis (Master's). University of Liege.

Lefas, I. D., Kotsovos, M. D. and Ambraseys, N. N., (1990). "Behavior of reinforced concrete structural walls: strength, deformation characteristics, and failure mechanism." *ACI Structural Journal*, 87(1), 23-31.

Liu, G. R., Song, Y. P. and Qu, F. L., (2010). "Post-fire cyclic behavior of reinforced concrete shear walls." *Journal of Central South University of Technology*, 17(5), 1103-1108.

Lopes, M. S., (2001). "Experimental shear-dominated response of RC walls. Part II: Discussion of results and design implications." *Engineering Structures*, 23(5), 564-574.

Luna, B. N., Rivera, J. P. and Whittaker, A. S., (2015). "Seismic behavior of low-aspect-ratio reinforced concrete shear walls." *ACI Structural Journal*, 112(5), 593-604.

Luna, B. N., (2016). "*Seismic response of low aspect ratio reinforced concrete walls for buildings and safety-related nuclear applications*." Thesis (Doctoral). State University of New York at Buffalo.

Maier, J. and Thürlimann, B., (1985). "*Bruchversuche an Stahlbetonscheiben* (Report No. 8003-1)." Zürich: Institut für Baustatik und Konstruktion der ETH Zürich. (in German)

Mazars, J., Kotronis, P. and Davenne, L., (2002). "A new modelling strategy for the behaviour of shear walls under dynamic loading." *Earthquake Engineering and Structural Dynamics*, 31(4), 937-54.

Mihaylov, B. I., Bentz, E. C. and Collins, M. P., (2013). "Two-parameter kinematic theory for shear behavior of deep beams." *ACI Structural Journal*, 110(3), 447-456.

Mihaylov, B. I., Hannewald, P. and Beyer, K., (2016). "Three-parameter kinematic theory for shear-dominated reinforced concrete walls." *Journal of Structural Engineering*, 142(7), 04016041.

Mihaylov, B. I., Liu, J. and Ozkan. M. F., (2021). "Modeling the effect of prestressing on ultimate shear behavior of deep-to-slender concrete beams." *ACI Structural Journal*, 118(2), 89-100.

Nie, X., Wang, J. J., Tao, M. X., Fan, J. S., Mo, Y. L. and Zhang, Z. Y., (2020). "Experimental study of shear-critical reinforced-concrete shear walls under tension-bending shear-combined cyclic load." *Journal of Structural Engineering*, 146(5), 04020047.

Oh, Y. H., Han, S. W. and Lee, L. H., (2002). "Effect of boundary element details on the seismic deformation capacity of structural walls." *Earthquake Engineering and Structural Dynamics*, 31(8), 1583-602.

Panagiotou, M., Restrepo, J. I., Schoettler, M. and Kim, G., (2012). "Nonlinear cyclic truss model for reinforced concrete walls." *ACI Structural Journal*, 109(2), 205-214.

Park, H. and Eom, T., (1995). "Truss model for nonlinear analysis of RC members subject to cyclic loading." *Journal of Structural Engineering*, 133(10), 1351-63.

Pilakoutas, K. and Elnashai, A. S., (1995). "Cyclic behavior of reinforced concrete cantilever walls, Part I: Experimental results." *ACI Structural Journal*, 92(3), 271-81.

Popovics, S., (1973). "A numerical approach to the complete stress-strain curve of concrete." *Cement and Concrete Research*, 3(5), 583-99.

Priestley, M. J. N., Calvi, G. M. and Kowalsky, M. J., (2007). "*Displacement-based seismic design of structures*." Pavia, Italy: IUSS Press.

Rong, X. L., Zheng S. S., Zhang Y. X., Zhang X. Y. and Dong L. G., (2020). "Experimental study on the seismic behavior of RC shear walls after freeze-thaw damage." *Engineering Structures*, 206, 110101.

Tatar, N. and Mihaylov B., (2021). "Kinematic-based modeling of shear-dominated concrete walls with rectangular and barbell sections." *Journal of Earthquake Engineering,* 25(7), 1408-1437.

Terzioglu, T., Orakcal, K. and Massone, L. M., (2018). "Cyclic lateral load behavior of squat reinforced concrete walls." *Engineering Structures*, 160, 147-60.

Tran, T. A. and Wallace, J. W., (2015). "Cyclic testing of moderate-aspect-ratio reinforced concrete structural walls." *ACI Structural Journal*, 112(6), 653-665.

Vecchio, F. J. and Collins, M. P., (1986). "The modified compression-field theory for reinforced concrete elements subjected to shear." *ACI Structural Journal*, 83(2), 219-231.

Vecchio, F. J., (2000). "Disturbed stress field model for reinforced concrete: Formulation." *Journal of Structural Engineering*, 126(9), 1070-1077.

Wiradinata, S., (1985). "*Behaviour of squat walls subjected to load reversals*." Thesis (Doctoral). Department of Civil Engineering, University of

Toronto.
Wu, S., Li, H., Wang, X., Li, R., Tian, C. and Hou Q., (2022). "Seismic performance of a novel partial precast RC shear wall with reserved cast-in-place base and wall edges." *Soil Dynamics and Earthquake Engineering*, 152, 107038.
Xiong, C., Chu, M., Liu, J. and Sun, Z., (2018). "Shear behavior of precast concrete wall structure based on two-way hollow-core precast panels." *Engineering Structures*, 176, 74-89.
Yuniarsyah, E., Kono, S., Tani, M., Taleb, R., Sugimoto K. and Mukai T., (2017). "Damage evaluation of lightly reinforced concrete walls in moment resisting frames under seismic loading." *Engineering Structures*, 132, 349-71.
Zhou, Y., Zheng, S., Chen, L., Long, L., Dong, L. and Zheng, J., (2021). "Experimental and analytical investigations into the seismic behavior and resistance of corroded reinforced concrete walls." *Engineering Structures*, 238, 112154.

Appendix: Example of 3PKT calculations

The following example is given for shear wall RF0 of (Franssen *et al*. 2021).

1) Geometry of the kinematic model

$$\alpha = \tan^{-1}(h/a_{cl}) = \tan^{-1}(1500/2300) = 33.1°$$

$$\alpha_1 = \max(\alpha, 30°) = 33.1°$$

$$A_s = \frac{1}{2}\rho_l bh/100 = \frac{1}{2}\times 1.75\times 230\times 1500/100 = 3020 \text{ mm}^2$$

$$\rho_{l1} = \frac{A_s}{b\cdot\left(h-d+\min\left[1.5(h-d), d-h/2\right]\right)}\times 100 = \frac{3020}{230\times\left(1500-1146+\min\left[1.5\times(1500-1146), 1146-1500/2\right]\right)}\times 100 = 1.75\%$$

$$s_{cr} = \frac{0.28\times d_b}{\rho_{l1}}\times 100 = \frac{0.28\times 16}{1.75}\times 100 = 256 \text{ mm}$$

$$l_0 = \max\left[s_{cr}, \min(1.5(h-d), d-h/2)\cdot\cot\alpha_1\right] = \max\left[256, \min(1.5\times(1500-1146), 1146-1500/2)\cdot\cot 33.1\right] = 607 \text{ mm}$$

$$l_k = l_0 + \min\left[s_{cr}, d\times\left(\cot\alpha - \cot\alpha_1\right)\right] = 607 + 0 = 607 \text{ mm}$$

$$l_t = d/\tan\alpha_1 + (l_k - l_0) = 1146/\tan 33.1 + (607-607) = 1757 \text{ mm}$$

$$l_{b1e} = \min\left(0.11\sqrt{a^2+h^2}, 370\right) = \min\left(0.11\sqrt{2550^2+1500^2}, 370\right) = 325 \text{ mm}$$

$$\alpha_F = \tan^{-1}(h/a) = \tan^{-1}(1500/2550) = 30.5°$$

$$\alpha_\Delta = \min\left(\frac{\alpha_F}{\alpha_1}\times 90, 90°\right) = \min\left(\frac{30.5}{33.1}\times 90, 90°\right) = 82.8°$$

$$\because \rho_{lw} = 1.75\% \geq 0.2\% \rightarrow n_{cr} = \frac{l_k}{s_{cr}} = 607.2/256 = 2.37$$

2) CLZ degrees of freedom and its shear strength

$$\Delta_{CLZ} = \frac{\varepsilon_{CLZ}\times 3l_{b1e}\cdot\cos\alpha_1}{\cos(\alpha_\Delta - \alpha_F)} = \frac{0.0035\times 3\times 325\times\cos 33.1}{\cos(82.8-30.5)} = 4.68 \text{ mm}$$

$$\Delta_c = \Delta_{CLZ}\sin\alpha_\Delta = 4.68\times\sin 82.8 = 4.65 \text{ mm}$$

$$\Delta_{cx} = \Delta_{CLZ}\cos\alpha_\Delta = 4.68\times\cos 82.8 = 0.5865 \text{ mm}$$

$$V_{CLZ} = l_{b1e}\times\sin\alpha_1\times b\times 1.48 f_c'^{0.8}\sin\alpha_F = 325.4\times\sin 33.1\times 230\times 1.48\times 52.3^{0.8}\sin 30.5/1000 = 727 \text{ kN}$$

3) First iteration $\rightarrow \varepsilon_{t,avg} = 0.00150$

Note: The contributions of the DOF Δ_{cx} in the calculations of the crack width w and transverse reinforcement strain ε_v are neglected for simplicity.

$$w = \left[\begin{array}{c}\left(\dfrac{\varepsilon_{t,avg} l_k h}{2\cdot\sin\alpha_1\cdot d}\right)\\ +\Delta_c\cos\alpha_1\end{array}\right]/n_{cr} = \left[\begin{array}{c}\left(\dfrac{0.0015\times 607\times 1500}{2\times\sin 33.1\times 1146}\right)\\ +4.65\times\cos 33.1\end{array}\right]/2.37 = 2.10 \text{ mm}$$

$$\varepsilon_v = 2.0\left[\begin{array}{c}\left(\dfrac{\varepsilon_{t,avg} l_t}{d}\right)\times 0.5 d_1\cot\alpha_1\\ +\Delta_c - \varepsilon_{t,avg}\dfrac{(0.5d_1\cot\alpha_1)^2}{d}\end{array}\right]/0.9d_1 = 2.0\left[\begin{array}{c}\left(\dfrac{0.0015\times 1757.2}{1146}\right)\times 0.5\times 1461\times\cot 33.1\\ +4.65 - 0.0015\times\dfrac{(0.5\times 1461\times\cot 33.1)^2}{1146}\end{array}\right]/\left(0.9\times 1461\right) = 0.00850$$

$$\upsilon_{ci} = \frac{0.18\sqrt{f_c'}}{0.31+24w/\left(a_g+16\right)} = \frac{0.18\sqrt{52.3}}{0.31+24\times 2.1/(16+16)} = 0.69 \text{ MPa}$$

$$V_{ci} = \upsilon_{ci}\cdot b\cdot d_1 = 0.69\times 230\times 1461/1000 = 232 \text{ kN}$$

$$f_v = \min(\varepsilon_v \times 2\times10^5, f_{yv}) = \min(0.0085\times2\times10^5, 578)$$
$$= 578 \text{ MPa}$$

$$V_s = \frac{\rho_v}{100} b \max\begin{pmatrix} d_1 \cot\alpha_1 - 1.5 l_{b1e} - \dfrac{dl_0}{d_1} \\ 0.5 d_1 \cot\alpha_1 \end{pmatrix} f_v$$

$$= \frac{0.07}{100} \times 230 \times \max\begin{pmatrix} 1461\times\cot 33.1 - 1.5\times325 - \dfrac{1146\times607}{1461} \\ 0.5\times1461\times\cot 33.1 \end{pmatrix} \times 578$$

$$V_s = 119 \text{ kN}$$

$$n_b = \frac{A_s}{\dfrac{\pi}{4} d_b^{\,2}} = \frac{3020}{\dfrac{\pi}{4}\times16^2} = 15$$

$$V_d = n_b \cdot f_y \left[1 - \left[\min(\frac{\varepsilon_{t,avg}}{f_y / E_s}, 1)\right]^2\right] \times \frac{d_b^{\,3}}{3 l_k}$$

$$= 15\times522\left[1 - \left[\min(\frac{0.0015}{522/\left(2\times10^5\right)}, 1)\right]^2\right] \times \frac{16^3}{3\times607.2}$$

$$= 11.8 \text{ kN}$$

$$V = V_{CLZ} + V_{ci} + V_s + V_d = 727 + 232 + 119 + 11.8$$
$$= 1089 \text{ kN}$$

$$z = \min\left(-0.6\times\frac{N}{f_c' \cdot b \cdot h} + 0.9, 0.9\right)\times d$$

$$= \min\left(-0.6\times\frac{1200\times1000}{52.3\times230\times1500} + 0.9, 0.9\right)\times1146$$

$$= 986 \text{ mm}$$

$$V_{eq} = \begin{bmatrix} \left(2\times10^5 A_s \varepsilon_{t,avg} \times z\right) \\ +N\times\left[h/2 - (d-z)\right] \end{bmatrix} / a$$

$$= \begin{bmatrix} (2\times10^5\times3020\times0.0015\times985.6) \\ +1200\times\left[1500/2 - (1146 - 985.6)\right] \end{bmatrix} / 2550$$

$$= 628 \text{ kN}$$

$$\text{Error} = 100\times\left|V_{eq} - V\right| / V_{eq} = 100\times\left|628 - 1089\right| / 628$$
$$= 74\%$$

4) Final iteration $\rightarrow \varepsilon_{t,avg} = 0.00330$

$w \approx 2.63$ mm, $\varepsilon_v \approx 0.0101$

$V_{CLZ} = 727$ kN, $V_{ci} = 191$ kN, $V_s = 119$ kN, $V_d = 0$ kN

$V = V_{CLZ} + V_{ci} + V_s + V_d = 727 + 191 + 119 + 0 = 1037$ kN

$V_{eq} = 1036$ kN

$\text{Error} = 100\times\left|V_{eq} - V\right| / V_{eq} \approx 0\%$